Opto-Electronic Science

ISSN 2097-0382 CN 51-1800/O4

Spatio-temporal isolator in lithium niobate on insulator

Haijin Huang, Armandas Balčytis, Aditya Dubey, Andreas Boes, Thach G. Nguyen, Guanghui Ren, Mengxi Tan and Arnan Mitchell

Citation: Huang HJ, Balčytis A, Dubey A, Boes A, Nguyen TG et al. Spatio-temporal isolator in lithium niobate on insulator. *Opto Electron Sci*, **2**, 220022(2023).

https://doi.org/10.29026/oes.2023.220022

Received: 21 November 2022; Accepted: 3 March 2023; Published online: 30 March 2023

Opto-Electronic Science

Article

March 2023, Vol. 2, No. 3

DOI: 10.29026/oes.2023.220022

Spatio-temporal isolator in lithium niobate on insulator

Haijin Huang[1]*, Armandas Balčytis[1], Aditya Dubey[1], Andreas Boes[1,2,3], Thach G. Nguyen[1], Guanghui Ren[1], Mengxi Tan[1] and Arnan Mitchell[1]*

In this contribution, we simulate, design, and experimentally demonstrate an integrated optical isolator based on spatiotemporal modulation in the thin-film lithium niobate on an insulator waveguide platform. We used two cascaded travelling wave phase modulators for spatiotemporal modulation and a racetrack resonator as a wavelength filter to suppress the sidebands of the reverse propagating light. This enabled us to achieve an isolation of 27 dB. The demonstrated suppression of the reverse propagating light makes such isolators suitable for the integration with III-V laser diodes and Erbium doped gain sections in the thin-film lithium niobate on the insulator waveguide platform.

Keywords: Isolator; lithium niobate; modulator

Huang HJ, Balčytis A, Dubey A, Boes A, Nguyen TG et al. Spatio-temporal isolator in lithium niobate on insulator. *Opto-Electron Sci* **2**, 220022 (2023).

Introduction

Thin-film lithium niobate on insulator (LNOI) is a photonic integrated circuit platform that has enabled breakthrough demonstrations such as optical frequency comb generation[1–3] and second harmonic generation[4–6] in recent years. These achievements are enabled by lithium niobate's standout material properties, which include a strong optical nonlinearity, its piezoelectricity, and the ability to achieve phase modulation with minimal amplitude modulation via the electro-optic effect[7]. Recently, light sources such as amplifiers[8] and lasers[9] have also been integrated with LNOI by using Erbium doping and the integration of III-V laser diodes[10]. Such integrated light sources are sensitive to back reflections, which can cause detrimental instabilities[11]. Reduction of the undesired feedback into the light sources to low enough levels so that they do not interfere with their operation can be achieved through the use of non-reciprocal devices such as optical isolators and circulators.

Nonreciprocal optical devices have been demonstrated in several other photonic integrated circuit platforms by using three main methods: magnetic biasing[12], optical nonlinearity[13], and spatiotemporal modulation[14]. Magnetic biasing is attractive due to its broadband nature but requires the integration of magneto-optical materials, which is a challenging fabrication process and can induce relatively high optical losses[15]. Optical nonlinear non-reciprocal devices possess an advantage in that they can be achieved monolithically in LNOI. However, their operation is dependent on the power of input light sources[13], which is not always desired. Isolators that use spatiotemporal modulation operate

[1]Integrated Photonics and Applications Centre, School of Engineering, RMIT University, Melbourne VIC 3001, Australia; [2]School of Electrical and Electronic Engineering, The University of Adelaide, Adelaide SA 5005, Australia; [3]Institute for Photonics and Advanced Sensing, The University of Adelaide, Adelaide SA 5005, Australia.

*Correspondence: HJ Huang, E-mail: s3582482@student.rmit.edu.au; A Mitchell, E-mail: arnan.mitchell@rmit.edu.au

Received: 21 November 2022; Accepted: 3 March 2023; Published online: 30 March 2023

independently of the optical power from the light source and appear to be an attractive way to achieve isolators in LNOI monolithically, by leveraging the excellent electro-optical modulation characteristics of LNOI[16].

In this contribution, we simulate, design, and experimentally demonstrate integrated isolators in the LNOI waveguide platform. The non-reciprocal operation is achieved by using spatiotemporal modulation of two cascaded travelling wave phase modulators. The microwave signal that was applied to the modulators was selected so that most of the optical power is transferred to the sidebands when the device is operated in the reverse direction. The sidebands are then suppressed by an integrated add-drop racetrack resonator, enabling us to demonstrate an optical isolation of 27 dB.

Device design

Figure 1(a) shows the schematic overview of our proposed integrated isolator in LNOI, which consists of two identical travelling wave phase modulators connected in series and an add-drop racetrack resonator for spectral filtering. Like the tandem phase modulator-based optical isolator in the silicon on the insulator waveguide platform[17], two phase modulators are modulated with two microwave signals having the same amplitude A but with a phase difference ϕ. In the forward direction, the output optical field after passing through the two modulators can be written as:

$$\begin{aligned} E_f &= E_{\rm o}{\rm e}^{{\rm i}\omega_c t}{\rm e}^{{\rm i}R_f\cos(2\pi f_s t+\phi)}{\rm e}^{{\rm i}R_f\cos(2\pi f_s(t+\Delta T))} \\ &= E_{\rm o}{\rm e}^{{\rm i}\omega_c t}{\rm e}^{{\rm i}2R_f\cos(2\pi f_s t+(2\pi f_s\Delta T+\phi)/2)\cos((2\pi f_s\Delta T-\phi)/2)}\ , \end{aligned} \tag{1}$$

where $E_{\rm o}$ and ω_c are the optical carrier's amplitude and angular frequency, ΔT is the time delay between the two modulators, $R_f = A/V_{\pi,f}$ is the modulation index, and $V_{\pi,f}$ is the modulator switching voltage for the forward direction. When the phase difference ϕ and the time delay ΔT satisfy the following condition:

$$2\pi f_s\Delta T - \phi = \pi + k\pi\ , \tag{2}$$

where k is an integer, the output field is identical to the input field for the forward direction, which means that the optical field is unchanged, regardless of the modulation signal power. However, when the light passes through the modulation area in reverse, the output optical field will be:

$$\begin{aligned} E_b &= E_{\rm o}{\rm e}^{{\rm i}\omega_c t}{\rm e}^{{\rm i}R_b\cos(2\pi f_s t)}{\rm e}^{{\rm i}R_b\cos 2\pi f_s((t+\Delta T)+\phi)} \\ &= E_{\rm o}{\rm e}^{{\rm i}\omega_c t}{\rm e}^{{\rm i}2R_b\cos\left(2\pi f_s t+\frac{2\pi f_s\Delta T+\phi}{2}\right)\cos((\phi+2\pi f_s\Delta T)/2)} \\ &= E_{\rm o}{\rm e}^{{\rm i}\omega_c t}\sum_{n=-\infty}^{n=+\infty}{\rm i}^n{\rm J}_n\left(2R_b\cos\left(\frac{\phi+2\pi f_s\Delta T}{2}\right)\right) \\ &\quad\cdot{\rm e}^{{\rm i}n\left(2\pi f_s t+\frac{2\pi f_s\Delta T+\phi}{2}\right)}\ , \end{aligned} \tag{3}$$

where R_b is the modulation index when the light is propagation in the reverse direction, ${\rm J}_n(x)$ represents the nth order Bessel function of the first kind. When operating in the reverse direction, the power of the optical carrier is transferred to the sidebands, and the remaining power in the carrier is proportional to ${\rm J}_n\left(2R_b\cos\left(\frac{\phi+2\pi f_s\Delta T}{2}\right)\right)$. The sidebands can be filtered out by the add-drop racetrack resonator, leaving only the carrier passing through. To ensure strong suppression of the carrier and transfer of most of the optical field to the sidebands, we need to operate the modulators for the reverse-propagating light such that the modulation index of the two modulators:

$$2R_b\cos\left(\frac{\phi+2\pi f_s\Delta T}{2}\right)\approx 0.77\pi\ , \tag{4}$$

which results in the carrier ${\rm J}_0\left(2R_b\cos((\phi+2\pi f_s\Delta T)/2)\right)\approx 0$. Combining Eq. (2) and Eq. (4), the conditions for isolation operation are[18]:

$$2\pi f_s\Delta T = \pi + k\pi + \phi \text{ and } R_b = \frac{0.77\pi}{2\sin\left(\frac{k\pi}{2}-2\pi f_s\Delta T\right)}\ . \tag{5}$$

In this work, we select $\phi=\pi/2$ and k=2, resulting in $\Delta T = 7/4f_s$ to minimize the requirement on the RF driving power[18].

The photonic waveguide platform that is used in this work to demonstrate the isolator is the silicon nitride-loaded LNOI[19,20]. A cross-section of the phase modulator is illustrated in Fig. 1(b). For the operation of the modulators, we chose a modulation frequency f_s =22.5 GHz and of delay time was $\Delta T = 7/4f_s$, which, for a group index of 2.23, corresponds to a waveguide length of 10.4 mm. When the modulators are driven with a π/2 phase difference, the simulated spectra for the forward and reverse propagating light can be seen in Fig. 1(c) and 1(d), respectively. One can see that for the forward direction, all of the optical power remains at the carrier wavelength, whereas in the reverse direction most of the optical power is transferred to the sidebands, while the power of the carrier wavelength (1550 nm) is strongly

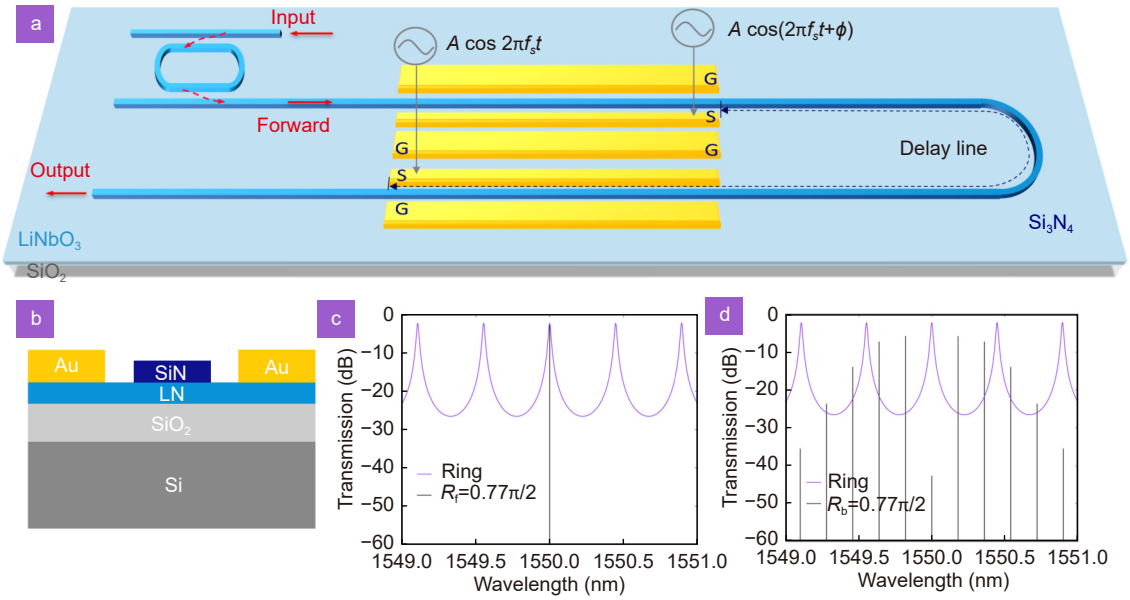

Fig. 1 | (**a**) Illustration of the investigated spatiotemporal isolator in LNOI. (**b**) Cross-section of the SiN loaded LNOI waveguide. (**c**) Purple curve shows the simulated spectral response of the add-drop racetrack resonator with an FSR of 55 GHz. Black line is the simulated spectral response for light propagating in the forward direction for a modulation index of 0.77π/2 when the device meets the condition of Eq. (2). (**d**) Black line is the simulated spectral response for the reverse direction assuming a modulation index of 0.77π/2. The response of the add-drop racetrack resonator is shown in (c) and (d) for reference and is not considered in the black curves.

reduced. To suppress the sidebands in the reverse direction we designed an add-drop racetrack resonator with a radius of 200 μm and a straight waveguide section length of 576 μm, resulting in a free spectral range of 55 GHz. For estimating the sharpness of the resonances of the racetrack resonator, we assumed a waveguide loss of 1 dB/cm. The expected add-drop filter transmission spectrum can be seen as the purple line in Fig. 1(c) and 1(d), which should result in the carrier being transmitted with minimal loss in the forward direction and be able to suppress most of the power in the sidebands in the reverse direction.

Experimental results and discussion

To experimentally demonstrate the designed isolator, we fabricated the device in the silicon nitride (SiN) loaded thin-film lithium niobate on insulator integrated waveguide platform. We ordered the wafers from NanoLN and chose X-cut LNOI, to make use of LN's strongest electro-optic tensor component r_{33}, for Y-propagating modulators. The details of the waveguide and electrode fabrication steps are outlined in our prior work[19]. An optical microscope image of the fabricated device is presented in Fig. 2(a), showing the input at the top left corner, which couples to an add-drop racetrack resonator before passing through the two cascaded phase modulators. The total length of the add-drop racetrack resonator is 2.4 mm. It has a 200 μm bending radius and a separation (edge to edge) of 1.05 μm between the bus waveguide and coupler. Using a racetrack resonator allows us to modify the coupling strength between the bus waveguide and the racetrack resonator by changing the length of the straight section of coupling region (without changing the coupling gap). It is worth noting that other resonator to bus waveguide coupling methodologies (such as Pulley coupler) could have been chosen for this demonstration without impacting the performance. An optical microscope image of the coupling region is shown in Fig. 2(b). For the modulator design, whose segment is presented in Fig. 2(c), the length of the travelling wave modulator is 7060 μm, with a 5.8 μm electrode gap and a 0.5 μm thick Au electrode. The width and height of the SiN loading waveguide, shown in the scanning electron microscopy (SEM) image in Fig. 2(d) is 1 μm and 0.3 μm respectively, resulting in single-mode operation at a 1550 nm wavelength, similar to our previous demonstrations[19].

To experimentally characterize the proposed isolator, we first investigated the filtering behavior of the racetrack cavity using a tunable laser. The drop-port transmission spectra of the racetrack resonator are shown as a blue line in Fig. 3(a). Afterwards, we

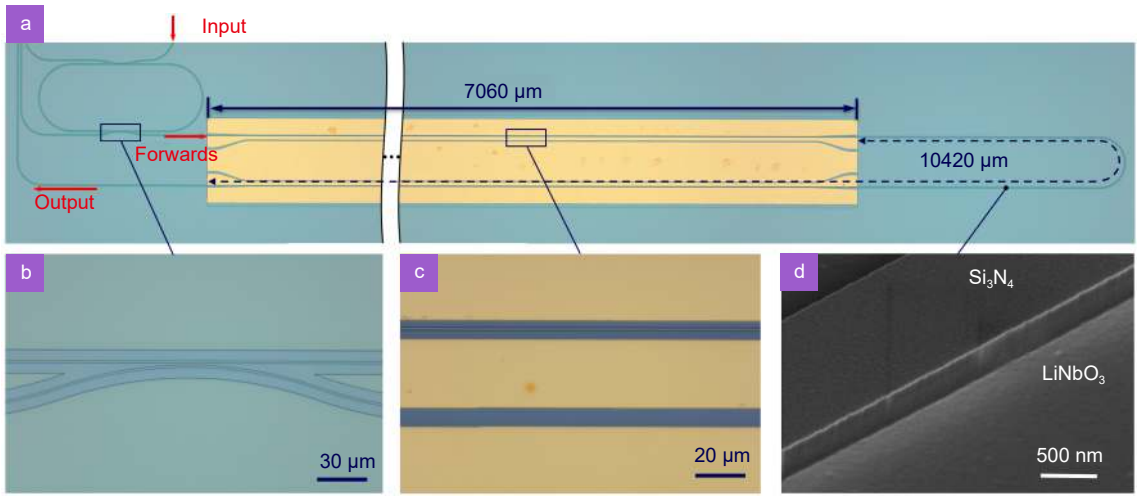

Fig. 2 | (**a**) Optical microscope image of the fabricated isolator. (**b**) Magnified view of the racetrack resonator coupling region. (**c**) The traveling wave electrode alignment to the waveguide. (**d**) SEM image of the fabricated SiN loaded LNOI waveguide.

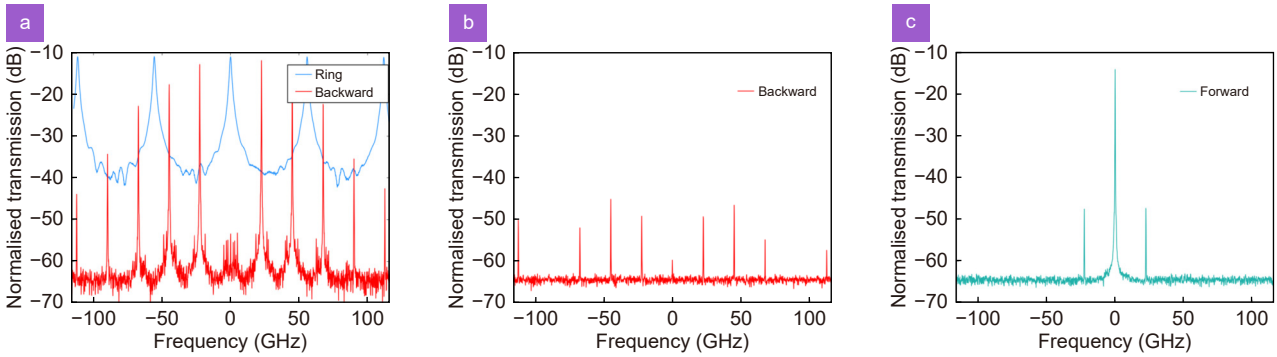

Fig. 3 | (**a**) The blue curve shows the measured transmission spectrum of the racetrack resonator. The red curve shows the measured spectrum of the cascaded phase modulators for light travelling in the reverse direction; Measured spectra of the isolator when operating the device in the (**b**) reverse direction and (**c**) forward direction, when using the racetrack resonator to suppress sidebands.

characterized the modulator without the racetrack resonator. For this, we coupled 1550 nm laser light such that we operate the device in a reverse direction and measured the spectra with a Finisar WaveAnalyzer 1500S High-Resolution Optical Spectrum Analyzer when a 22.5 GHz sinusoidal and cosine signal with the same power from an arbitrary waveform generator (Keysight M9505A) is applied to respective traveling wave electrodes. The microwave signals were injected in the direction of on-chip reverse propagating light, such that the reverse propagating light experiences the stronger modulation due to being velocity matched. On the opposite side of the traveling wave electrodes, microwave signals were terminated using 50 Ω impedance matching resistors. The power of the modulating RF signals was adjusted until the power of the carrier was minimal. In Fig. 3(a), the red curve shows the spectra for the reverse propagating light when 20.4 dBm microwave power is applied onto both modulators. One can see that the optical power in the carrier has been suppressed and most of the power has been transferred to the sidebands.

To validate the isolator operation and characterize the effectiveness of the racetrack resonator in suppressing the undesired optical power in the sideband, we aligned the laser wavelength so that it is on resonance with the racetrack resonator and analyzed reverse-propagating light output at the drop port. The spectrum of the filtered light is shown in Fig. 3(b). Compared to Fig. 3(a) one can see that the sidebands are strongly suppressed through spectral filtering with the racetrack resonator.

Next, we measured the spectra when operating the optical isolator in the forward direction and passing the light through the racetrack resonator (when operating on resonance) with the same RF modulation signals as in the reverse direction. The spectrum is shown in Fig. 3(c). One can see that in this case most of the optical power remains confined in the carrier and only minimal power is transferred to the sidebands and the extra spectral

Table 1 | Comparison of isolators performance that uses spatiotemporal modulation and operates a C-band wavelength.

Year	Platform	Method	Isolation(dB)	Insertion loss (dB)	Ref
2022	LNOI	2 cascaded phase modulators and spectral filtering with racetrack resonator	27	10	This work
2021	Si	Microring modulators, phase shifter and bandpass filter	13	18	ref.[22]
2014	Si	Tandem phase modulator in long interferometer	3	11.1	ref.[23]
2012	Si	Interbrand photonic transition in a modulated, slotted waveguide	3	70	ref.[24]
2011	InP	2 cascaded modulators	11	2.3	ref.[17]
2005	GaAs-AlGaAs	Single sideband electro-optical modulator	30	8	ref.[25]

components can be filtered out by another racetrack resonator or filter. The incomplete suppression of the sidebands is likely caused by the imbalance in the modulation index applied to the two modulators due to the different modulation efficiencies of the phase modulators as a result of fabrication tolerances (e.g., waveguide to electrode alignment). To quantify the isolation strength, we also measured the power difference with an optical power meter when operating the isolator in the forward and reverse directions, resulting in an isolation of 27 dB.

The insertion loss of the isolator is ~10 dB, which include 3.2 dB of loss by the racetrack resonator (not operating it perfectly at critical coupling condition), 4.5 dB of propagating loss (1.5 dB/cm loss for a 29.7 mm long waveguide) and 2.3 dB of loss due to additional scatter, which may have been caused by slight misalignment and defects of the modulator electrodes. This shows that the insertion loss can be significantly improved by: (i) using waveguides with lower propagation loss, (ii) operating add-drop racetrack resonator at the critical coupling condition and (iii) ensuring that the electrodes do not cause additional waveguide losses due to overlap of the optical mode with the electrodes. If these aspects of the device are improved, the insertion loss of the device can readily be reduced to <3 dB.

It is important to note that the experimental results for operating the fabricated device in reverse direction showed that after filtering the carrier contains less power than the filter-suppressed sidebands. This indicates that the experimentally achieved 27 dB isolation of the device is currently limited by the suppression of the sidebands, which can be improved by having sharper resonances by using higher-quality factor resonators or cascaded ring resonators. One disadvantage of sharper resonances is that the operation wavelength of the light sources needs to align with the resonance wavelength of the racetrack resonator, making it exceedingly narrowband. However, additional versatility can be attained by tuning the resonance wavelength of the racetrack resonator using heaters and locking it to the laser wavelength.

One limitation of the presented isolator is the relatively long length of the waveguide, which can be prohibitive for certain applications. In the current design, the length of delay line is mainly depending on the length of the EO modulator and the modulation frequency. Compact modulators such as demonstrated in ref.[21] and higher modulation frequencies can help to reduce the size of the isolator.

In Table 1 we compare the isolator performance demonstrated in this work with spatio-temporal isolator demonstration in the literature, across different waveguide platforms. One can see that the demonstrated isolation is one of the highest ones, while insertion loss requires improvements to be competitive. If the recommendations to reduce the insertion loss to <3 dB are implemented, it would make the proposed spatio-temporal isolator attractive for co-integration with light sources on the LNOI waveguide platform.

Conclusion

In this work, we designed and experimentally demonstrated an integrated isolator that is based on spatiotemporal modulation with 27 dB isolation in the LNOI waveguide platform. This was achieved by using LN's excellent electro-optic modulation properties and suppressing the optical power in the sidebands with a racetrack resonator filter. The isolation ratio of our device was limited by the racetrack resonator, providing scope for further improvements in the near future, making the demonstrated isolator suitable for future applications such as LNOI circuits with integrated light sources and amplifiers.

References

1. Zhang M, Buscaino B, Wang C, Shams-Ansari A, Reimer C et al. Broadband electro-optic frequency comb generation in a lithium niobate microring resonator. *Nature* **568**, 373–377 (2019).
2. Xu MY, He MB, Zhang HG, Jian J, Pan Y et al. High-performance coherent optical modulators based on thin-film lithium

niobate platform. *Nat Commun* **11**, 3911 (2020).
3. Wang C, Zhang M, Yu MJ, Zhu RR, Hu H et al. Monolithic lithium niobate photonic circuits for Kerr frequency comb generation and modulation. *Nat Commun* **10**, 978 (2019).
4. Lu JJ, Surya JB, Liu XW, Bruch AW, Gong Z et al. Periodically poled thin-film lithium niobate microring resonators with a second-harmonic generation efficiency of 250, 000%/W. *Optica* **6**, 1455–1460 (2019).
5. Ma JJ, Xie F, Chen WJ, Chen JX, Wu W et al. Nonlinear lithium niobate metasurfaces for second harmonic generation. *Laser Photonics Rev* **15**, 2000521 (2021).
6. Fedotova A, Younesi M, Sautter J, Vaskin A, Löchner FJF et al. Second-harmonic generation in resonant nonlinear metasurfaces based on lithium niobate. *Nano Lett* **20**, 8608–8614 (2020).
7. Wooten EL, Kissa KM, Yi-Yan A, Murphy EJ, Lafaw DA et al. A review of lithium niobate modulators for fiber-optic communications systems. *IEEE J Sel Top Quantum Electron* **6**, 69–82 (2000).
8. Zhou JX, Liang YT, Liu ZX, Chu W, Zhang HS et al. On‐chip integrated waveguide amplifiers on erbium‐doped thin‐film lithium niobate on insulator. *Laser Photonics Rev* **15**, 2100030 (2021).
9. Luo Q, Yang C, Zhang R, Hao ZZ, Zheng DH et al. On-chip erbium-doped lithium niobate microring lasers. *Opt Lett* **46**, 3275–3278 (2021).
10. Snigirev V, Riedhauser A, Lihachev G, Riemensberger J, Wang RN et al. Ultrafast tunable lasers using lithium niobate integrated photonics. arXiv: 2112.02036 (2021). https://doi.org/10.48550/arXiv.2112.02036
11. Tang LW, Li JC, Yang SG, Chen HW, Chen MH. A method for improving reflection tolerance of laser source in hybrid photonic packaged micro-system. *IEEE Photonics Technol Lett* **33**, 465–468 (2021).
12. Levy M, Osgood RM, Hegde H, Cadieu FJ, Wolfe R et al. Integrated optical isolators with sputter-deposited thin-film magnets. *IEEE Photonics Technol Lett* **8**, 903–905 (1996).
13. Kittlaus EA, Weigel PO, Jones WM. Low-loss nonlinear optical isolators in silicon. *Nat Photonics* **14**, 338–339 (2020).
14. Sounas DL, Alù A. Non-reciprocal photonics based on time modulation. *Nat Photonics* **11**, 774–783 (2017).
15. Srinivasan K, Stadler BJH. Review of integrated magneto-optical isolators with rare-earth iron garnets for polarization diverse and magnet-free isolation in silicon photonics [Invited]. *Opt Mater Express* **12**, 697–716 (2022).
16. Wang C, Zhang M, Chen X, Bertrand M, Shams-Ansari A et al. Integrated lithium niobate electro-optic modulators operating at CMOS-compatible voltages. *Nature* **562**, 101–104 (2018).
17. Doerr CR, Dupuis N, Zhang LM. Optical isolator using two tandem phase modulators. *Opt Lett* **36**, 4293–4295 (2011).
18. Lin Q, Wang JH, Fan SH. Compact dynamic optical isolator based on tandem phase modulators. *Opt Lett* **44**, 2240–2243 (2019).
19. Huang HJ, Han X, Balčytis A, Dubey A, Boes A et al. Non-resonant recirculating light phase modulator. *APL Photonics* **7**, 106102 (2022).
20. Boes A, Corcoran B, Chang L, Bowers J, Mitchell A. Status and potential of lithium niobate on insulator (LNOI) for photonic integrated circuits. *Laser Photonics Rev* **12**, 1700256 (2018).
21. Pan BC, Cao HY, Huang YS, Wang Z, Chen KX et al. Compact electro-optic modulator on lithium niobate. *Photonics Res* **10**, 697–702 (2022).
22. Dostart N, Gevorgyan H, Onural D, Popović MA. Optical isolation using microring modulators. *Opt Lett* **46**, 460–463 (2021).
23. Doerr CR, Chen L, Vermeulen D. Silicon photonics broadband modulation-based isolator. *Opt Express* **22**, 4493–4498 (2014).
24. Lira H, Yu ZF, Fan SH, Lipson M. Electrically driven nonreciprocity induced by interband photonic transition on a silicon chip. *Phys Rev Lett* **109**, 033901 (2012).
25. Bhandare S, Ibrahim SK, Sandel D, Zhang HB, Wust F et al. Novel nonmagnetic 30-dB traveling-wave single-sideband optical isolator integrated in III/V material. *IEEE J Sel Top Quantum Electron* **11**, 417–421 (2005).

Acknowledgements

This work was supported by the Australian Research Council (ARC) grants DP190102773, DP190101576, DP220100488. The authors acknowledge the facilities and the scientific and technical assistance of the Micro Nano Research Facility (MNRF) and the Australian Microscopy & Microanalysis Research Facility at RMIT University. This work was performed in part at the Melbourne Centre for Nanofabrication (MCN) in the Victorian Node of the Australian National Fabrication Facility (ANFF).

Competing interests

The authors declare no competing financial interests.